第 34 卷第 1 期
2018 年 1 月

无 机 化 学 学 报
CHINESE JOURNAL OF INORGANIC CHEMISTRY

Vol.34 No.1
206-214

水热法制备 Pr 掺杂 Bi_2WO_6 三维花状微球的光催化性能

张雅恒[1] 田 浩[1,2] 翟仁凯[1] 李建鑫[1] 顾大国[1] 强桂红[1] 奚新国*[,1,2]

([1]盐城工学院,材料科学与工程学院,盐城 224051)

([2]江苏省生态建材与环保装备协同创新中心,盐城 224051)

摘要：通过水热法制备稀土 Pr 掺杂 Bi_2WO_6 三维花状微球,利用 XRD、SEM、N_2 吸附–脱附、紫外–可见吸收光谱和光致发光光谱对所制备的光催化材料进行表征。通过降解亚甲基蓝评价样品的光催化活性。结果表明,1.0%Pr-Bi_2WO_6 样品的可见光催化活性最佳,降解率达到 95%。Pr 掺杂提高了催化剂的可见光吸收性能并且能够束缚光生电子使得电子空穴对有效分离从而获得强氧化物质。对其光催化降解做出了合理的解释。

关键词：Pr-Bi_2WO_6；稀土；荧光；光催化

中图分类号：O472+8 **文献标识码**：A **文章编号**：1001-4861(2018)01-0206-09

DOI:10.11862/CJIC.2018.013

Photocatalytic Activities of Pr Doped Bi_2WO_6 Three-Dimensional Flower Microspheres via Hydrothermal Method

ZHANG Ya-Heng[1] TIAN Hao[1,2] ZHAI Ren-Kai[1] LI Jian-Xing[1]

GU Da-Guo[1] QIANG Gui-Hong[1] XI Xin-Guo*[,1,2]

([1]*College of Materials Science and Engineering, Yancheng Institute of Technology, Yancheng, Jiangsu* 224051, *China*)

([2]*Jiangsu Collaborative Innovation Center for Ecological Building Materials and Environmental Protection Equipments, Yancheng, Jiangsu* 224051, *China*)

Abstract: The rare-earth Pr doped Bi_2WO_6 three-dimensional flower microspheres were synthesized by hydrothermal method. The prepared sample was investigated by X-ray diffraction, scanning electron microscopy, nitrogen adsorption-desorption, UV-Vis absorption spectroscopy and photoluminescence spectroscopy. The photocatalytic activity was evaluated by degrading of methylene blue. The results show that the 1.0% Pr-Bi_2WO_6 exhibits an enhanced visible light-induced photoactivity with the degradation rate of 95%. The Pr doping favors the absorption of visible light and trapping of electrons, thus the separation of electron-hole pairs is implemented effectivly and achieved strong oxidative species. This work provided a new photocatalyst with high-performance and a reasonable explanation of photocatalytic degradation.

Keywords: Pr-Bi_2WO_6; rare-earth; luminescence; photocatalyst

收稿日期:2017-07-10。收修改稿日期:2017-10-31。

教育部留学回国人员科研启动基金、国家重点研发计划项目(No.2016YFC0209202)、国家自然科学基金(No.51772258)、江苏省高校自然科学基金(No.15KJA430007)、江苏省生态建材与环保装备协同创新中心(No.CP201502,GX2015102)、江苏省自然科学基金(No.BK20140472)和江苏省高校大学生创新创业训练计划(No.201610305002Z)资助。。

*通信联系人。E-mail:xxg@ycit.cn

0 Introduction

Environmental problems related to organic pollutants bring severe threats to sustainable development of human[1-2]. Photocatalysis is expected to be an ideal green technology for several environmental areas and especially for the sustainable management of serious waste materials[3]. Undoubtedly, the semiconductor TiO_2 is known as one of the most excellent photocatalysts for the redox decomposition of a range of organic pollutants. However, TiO_2 has a wide band gap of 3.2 eV, which can be only in response to UV light but not to visible light that covers 43% of the sunlight. So it is important to develop visible-light-driven photocatalysts to efficiently utilize the solar light in the visible region. As one of the simplest Aurivillius oxides, Bi_2WO_6 has been found to be an excellent photocatalyst for degradation of organic compounds under UV and visible light irradiation due to its narrow band gap (2.6~2.8 eV)[4]. However, pure Bi_2WO_6 only presents photo absorption properties from the UV light region to visible light shorter than 450 nm, which reduces the efficiency of sunlight utilization.And its application also remains limited because of its high electron-hole recombination rate in photocatalytic process. In order to improve the photocatalytic capacity, doping strategy has been adopted widely. The doping may provide well-controlled ways to modify the structures, morphologies, surface features, and improve the separation efficiency of photoelectrons and holes, thus improve the photocatalytic capacity[5]. In addition to the ordinary common ion doping modification, the rare earth ions brought a new opportunity for the utilization of long-wavelength sunlight. As a host material for rare earth ions doping, Bi_2WO_6 has received more and more attention[6].

Recently, rare-earth doping has been demonstrated to be an efficient method for the enhancement of photocatalytic activity[7-8]. Yb^{3+}/Er^{3+} co-doped Bi_2WO_6 nanosheets exhibit higher photocatalytic activity than the undoped materials[9]. These reports have proved that the doping of rare earth ions can enhance the photocatalytic activity of Bi_2WO_6 with different explanations of catalytic mechanisms.

Yet until now, few literatures were concerned with Pr^{3+} modification on Bi_2WO_6. Especially, the photocatalytic material of Pr-Bi_2WO_6 has not been reported yet. In this paper, we first successfully prepared series of Pr-Bi_2WO_6 through hydrothermal process. The photo-catalytic activities of the Pr-Bi_2WO_6 were evaluated by degradation of methylene blue (MB) under visible light with excellent photo-degradation performances. The effects of Pr modification on the structure, optical properties, and visible light photocatalytic activities of Bi_2WO_6 catalysts were investigated and discussed in details.

1 Experimental

Preparation: The reagents used in experiment were AR grade and without further treatment. Pr-Bi_2WO_6 was prepared through a facile one-step hydrothermal process. The routes: 2.5 mmol of $Na_2WO_4 \cdot 2H_2O$ with appropriate amount of $Bi(NO_3)_3 \cdot 5H_2O$ and $Pr(NO_3)_3$ were blended in 50 mL volumes of deionized water and vigorously stirred for 30 min (n_W:(n_{Bi}+n_{Pr})=1:2). A series of Pr-doped Bi_2WO_6 samples (n_{Pr}:n_W= 0%, 0.5%, 1% and 2%) were prepared. After stirring for 30 min, the result yellow suspensions were added into 100 mL Teflon-lined stainless autoclave and heated at 180 ℃ for 24 h, then cooled to room temperature naturally. The products were washed with several times by deionized water and ethanol and dried at 60 ℃. Finally, the as-prepared samples of Pr-Bi_2WO_6 were achieved.

Characterization: The X-ray diffraction (XRD) experiments were carried out using a D/max-2400 diffractometer (Rigaku, Japan) operated at 40 kV, 40 mA, Cu $K\alpha$ radiation (λ=0.154 06 nm) with 2θ range of 10°~80°. The surface morphology of the as-obtained samples was examined using scanning electron microscopy (SEM, Hitachi S-4800, 20 kV). The Brunauer-Emmett-Teller (BET) specific surface area and Barrett-Joyner-Halenda (BJH) pore distribution of the samples were measured using a Micromeritics ASAP 2020-Minstru-ment. A Varian Cary 5000 UV-Vis

spectrophotometer was used to examine the UV-Vis diffuse reflectance spectra (DRS) of the samples. The emission spectra of all the samples were obtained using photoluminesce-nce measurement (PL, Jasco FP-6500) with a laser excitation source at 268 nm and recorded at a range from 300 to 550 nm. The photoresponses of the photocatalysts with or without visible light were examined at 0 V, which was equipped with a 150 W xenon lamp as the light source.

Photocatalytic experiment: The sample was submerged in the MB solution (10 mg·L^{-1}, 250 mL). Before irradiation, the solution was stirred in the dark for 40 min to ensure the establishment of adsorption-desorption equilibrium. A 300 W Xe lamp (visible light with a cutoff filter of 420 nm) was employed for the irradiation source and positioned 10 cm away from the reactor. The concentration of MB solution at some points was analyzed by measuring the light absorption of clear MB solution at 664 nm using a spectrophotometer. The percentage of degradation was calculated by C/C_0 (C is the concentration of remaining MB solution at each irradiated time interval (20 min), C_0 is the initial concentration).

2 Results and discussion

2.1 Texture analysis

The crystallinity and phase purity of the products were examined by XRD. As can be seen in Fig.1(a), the XRD patterns of the Pr doped Bi_2WO_6 samples are consistent with that of orthorhombic Bi_2WO_6 (PDF No. 39-0256)[10-11]. When the doping concentration below 1.5%, the strong diffraction peaks of (131), (200), (202), (133) and (262) planes are clearly observed and no any impunity diffraction peaks are observed. It indicates that the doping Pr does not change the crystal structure of Bi_2WO_6 and be a good evidence for no new phase formation with Pr doping. However, when the doping concentration of Pr increases to 1.5% or 2.0%, some other weak peaks appear beside the main peaks of Bi_2WO_6, which do not belong to the Bi_2WO_6 from Fig.1(a). It could belong to the phase of impurity peaks such as $Pr_xBi_{2-x}WO_6$[12]. Fig.1(b) shows the illustration of a 2×2×1 supercell (Bi_2WO_6) for modeling a single dopant in bulk Bi_2WO_6 (space group $Pca2_1$, No.29). One possible position of Bi atom is substituted by rare-earth Pr ion.

To further investigate the crystal structure change of the products, a careful comparison of the diffraction peak in (131) plane was shown in Fig.1(c) when the value of 2θ is from 26° to 30°. Results reveal that with the increase of Pr content, the peak position of (131) plane shifts slightly toward a lower 2θ value in XRD pattern. Moreover, the same phenomenon can be observed in other diffraction peaks. The lattice parameter can be determined by Eq.(**1**).

$$d_{hkl}=\frac{1}{\sqrt{\left(\frac{h}{a}\right)^2+\left(\frac{k}{b}\right)^2+\left(\frac{l}{c}\right)^2}} \quad (1)$$

Where d_{hkl} is the distance between crystal planes of (h k l), a, b and c are the lattice parameter of crystal. It has been found that the lattice parameter a increases gradually with the increase of doping Pr. This change

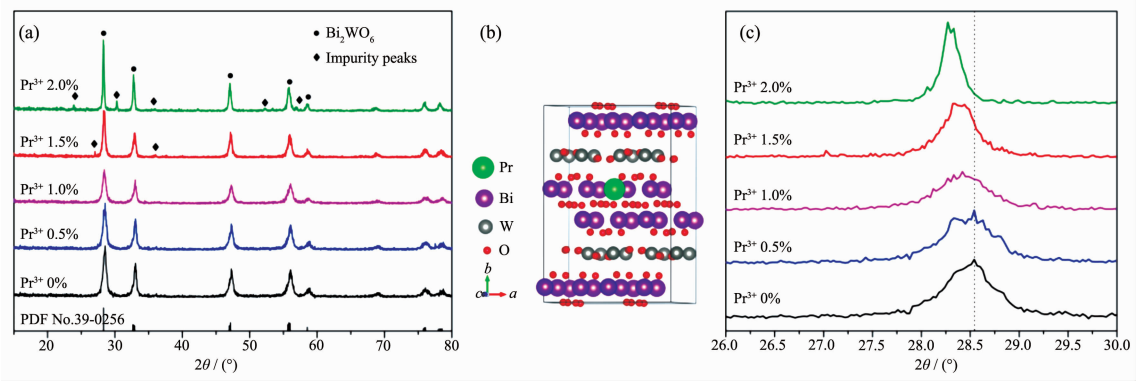

Fig.1 (a) XRD patterns of samples synthesized with different Pr contents; (b) Illustration of a 2×2×1 supercell of Pr-Bi_2WO_6; (c) Diffraction peak positions of the (131) plane

in lattice parameter could be due to the difference of ionic radius before and after ion substitute. The ionic radius of Pr^{3+} is larger than that of Bi^{3+}. Therefore, because of the substitution of Bi^{3+} by Pr^{3+}, Bi_2WO_6 would produce large lattice distortion and more lattice expansion. These results confirm that Pr ions have been successfully substituted into the Bi_2WO_6 lattices and it does not cause any additional phase.

2.2 Morphology

Fig.2 shows SEM images of different samples of 1.0%Pr-Bi_2WO_6, which can illustrate the characteristic types of larger-scale microstructures. When the sample of Pr-Bi_2WO_6 was prepared at 120 ℃, it can be seen that this sample is dense and composed of particles with size of around 1 μm (Fig.2(a)). In contrast, Fig.2 (b ~d) show completely different microstructures for the other sample prepared at 140, 160 and 180 ℃, respectively. From these images, it can be found that the sample looks like three-dimensional flower microspheres which are composed by irregular nanosheets. And Fig.2(d) shows that the particles of as-prepared sample are uniform and integrate. The sample of Pr-Bi_2WO_6 prepared at 200 ℃ shows a dense microstructure from the Fig.2(e). A comparison of the single particles prepared at 180 and 200 ℃ was carried out in the Fig.2(f). It is found that the accumulation angle of nano flake was changed due to the different temperature of preparation. From the SEM images, it is clear that flower microspheres is composed of cross flakes. The microspheres prepared at 180 ℃ have larger and more apparent pores. And then, it can be inferred these sample have better adsorption properties than other temperatures of preparation, so that they can provide larger specific surface area for the subsequent photocatalysis[13].

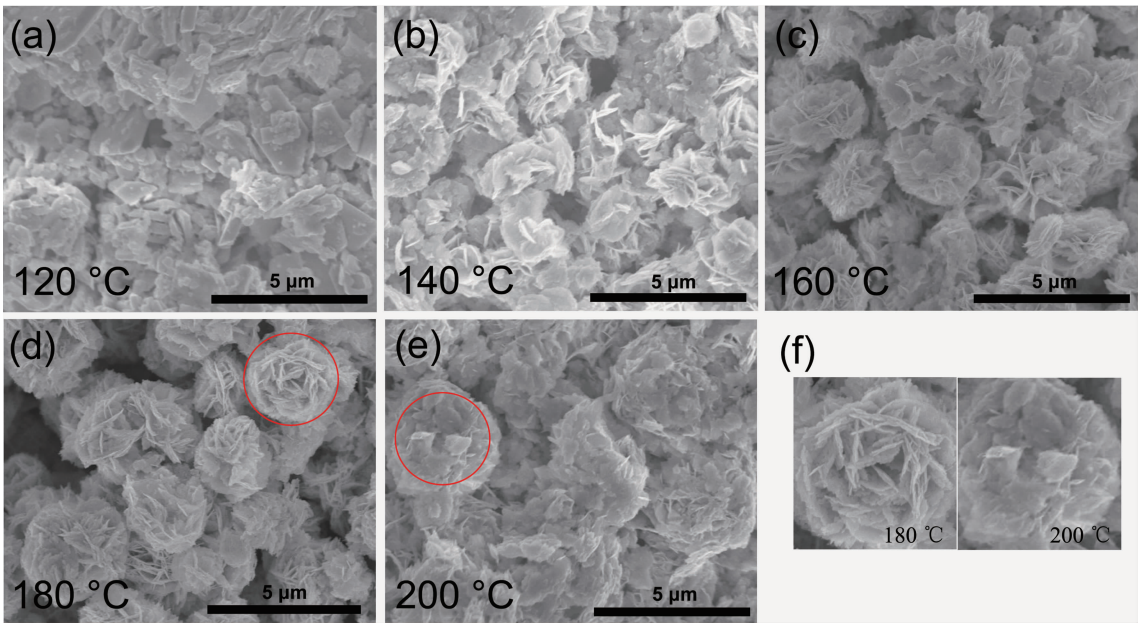

Fig.2　SEM images of Pr-Bi_2WO_6 prepared at different temperatures

2.3 Adsorption experiments

The adsorption experiments of Pr-Bi_2WO_6 samples were evaluated by testing the adsorption of MB. The suspension was stirred for 40 min in the dark to reach the adsorption-desorption equilibrium. The adsorption-desorption equilibriums of MB are shown in the Fig.3. It is found that all of the adsorption of dyes occurs within 30 min, and the as-prepared sample of 1.0%Pr-Bi_2WO_6 prepared at 180 ℃ exhibits the highest adsorption property than others, which can be due to the high surface area that increases the adsorption of dye molecules. The higher adsorption of dyes can lead to the easier and faster process of photocatalytic degradation, because photocatalytic reactions are typically surface-based processes and the photocatalytic efficiency is closely related to the adsorption

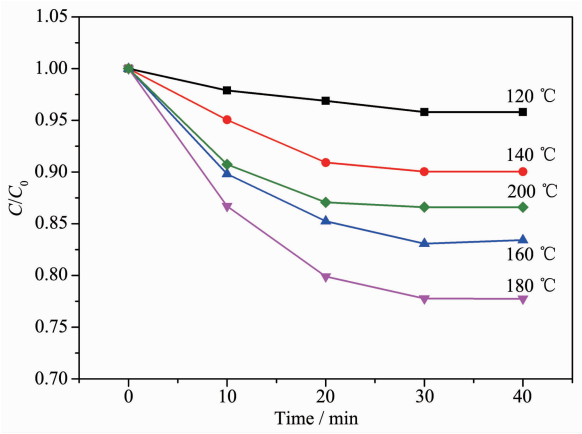

Fig.3 Adsorption properties experiments of different samples in the darkness

property of dyes on the surfaces of photocatalysts[14-15].

The porous structure is considered to be one of the most important factors on the photocatalytic activity of the samples synthesized by our modified method and characterized in detail. The N_2 adsorption -desorption isotherms of the as-prepared samples of 1.0%Pr-Bi_2WO_6 are presented in Fig.4(a). It can be seen that all the as-prepared samples show a type H3 hysteresis loop according to IUPAC classification[16], indicating the presence of mesopores (2~50 nm). Meanwhile, the areas of the hysteresis loops become largest when the temperature of hydrothermal treatment was at 180 ℃, which indicates that more porous structure could be obtained. Fig.4(b) shows the corresponding BJH pore size distributions of the samples. Considering the morphology of the three-dimensional flower observed in Fig.2, the smaller pores (<50 nm) could correspond to the pores inside the nanosheets[17]. From Fig.2, the aggregation of the nanosheets was larger than 100 nm. The peaks of pore size distributions can be observed from these three samples around 4 nm. As the inset shown in Fig.4(a), the BET surface area and pore volume of the samples prepared at 180 ℃ were the largest than others. This result is consistent with the results of the SEM and the adsorption experiments.

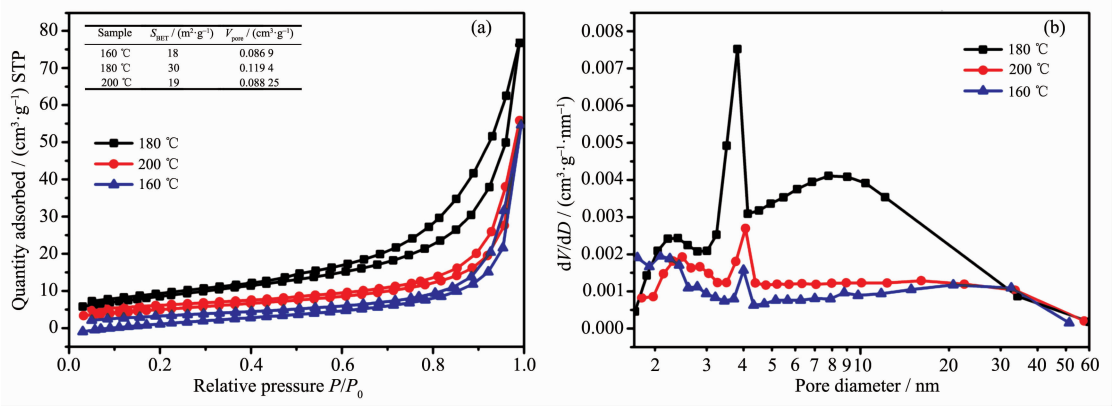

Fig.4 (a) N_2 adsorption-desorption isotherms and (b) BJH pore size distributions from desorption branch for samples of 1.0%Pr-Bi_2WO_6 prepared at different temperatures

2.4 UV-Vis diffuse reflectance spectroscopy and PL measurement

The optical properties of Pr doped Bi_2WO_6 samples as well as pure Bi_2WO_6 were probed by UV-Vis diffuse reflectance spectroscopy (DRS). Fig.5(a) shows the UV-Vis DRS of different samples. It shows that the absorption edge of pure Bi_2WO_6 is at about 450 nm. The doping of Pr^{3+} makes the absorption edges of the samples shift to longer wavelength region than that of pure Bi_2WO_6. The different Pr doped Bi_2WO_6 samples almost show the same absorption edge, at around 485 nm. The band gap width of materials can be estimated through Tauc formula[18-19]. As shown in Fig.4(b), the bandgap of pure Bi_2WO_6 is estimated as 2.71 eV. The bandgaps of 1.0% Pr doped Bi_2WO_6 sample is 2.56 eV, which is lower than that of pure Bi_2WO_6 crystal. These results indicate that the optical adsorption ability of Pr doped Bi_2WO_6 samples become much stronger within the scope of visible light.

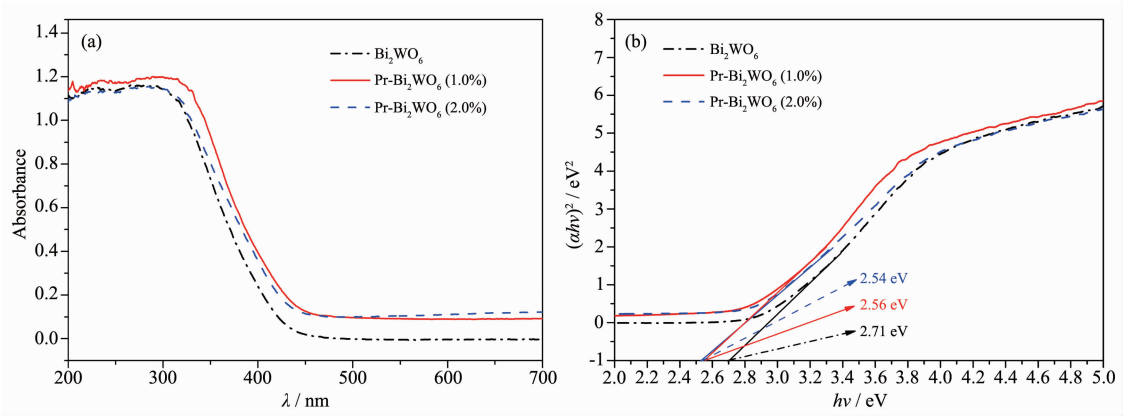

Fig.5　(a) UV-Vis DRS of different samples; (b) Bandgap energy of different samples estimated from the absorption edge

The electron-hole pairs′ recombination rate of Pr-Bi_2WO_6 was investigated using a photoluminescence measurement. The PL signals of semiconductor materials result from the recombination of photo-induced charge carriers[20]. So the emission intensity with lower value means less recombination of electron-hole pairs, and then can be benefical to the improvement of the photocatalytic activity[21]. Fig.6 shows the PL emission spectra of different doping quantities of Bi_2WO_6 powders with excitation wavelength of 268 nm. It can be seen that their photoluminescence displays the main peaks at the same of position but with different intensities. When the Pr doing amount was 1.0%, the intensity of excitonic PL signal was lowest. It implies that surface defects decrease and the recombination of photo-induced electrons and holes are inhibited. Three-dimensional flower microspheres can absorb more photon energy due to multiple scattering. Besides, the larger surface area offered by the flower-like configuration is available for generated charge carriers to undergo an electron transfer at the interface and beneficial to dye absorption[3].

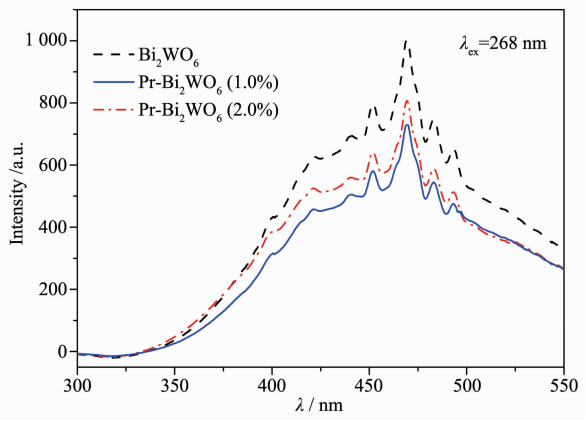

Fig.6　Photoluminescence spectra of Pr-Bi_2WO_6 after treatment with excitation wavelength of 268 nm

2.5　Photocatalytic performance test

Fig.7(a) shows UV-Vis spectral changes of MB with 1.0%Pr-Bi_2WO_6 as photocatalyst and exposure to Xe lamp irradiation for various durations. The adsorption is apparent during −40 to 0 min before turning on the Xe lamp (in the dark). Then, it can be seen that characteristic absorption of MB decreased rapidly with extension of the exposure time, and completely disappeared after about 80 min.

Fig.7(b) shows the photocatalytic degradation of MB with the different catalysts under irradiation with visible light for 80 min. It can be seen from the picture the absorbance of pure Bi_2WO_6 (120, 160, 200 ℃) as the photocatalyst has little change after 80 min with visible-light irradiation. With the doping amount of Pr increased to 1.0%, the photoactivity of Bi_2WO_6 increases significantly and it displays the highest degradation efficiency. About 95% MB can be removed in 80 min. When the doping content of Pr further increases to 1.5% or 2%, its photoactivity did not increase but decrease. The result of MB degradation under visible light in all samples suggest a higher photocatalytic activity with 1.0%Pr-Bi_2WO_6, which is in good agreement with the lowest PL intensity of the sample.

In order to determine the degree of mineralization reached during the photocatalysis

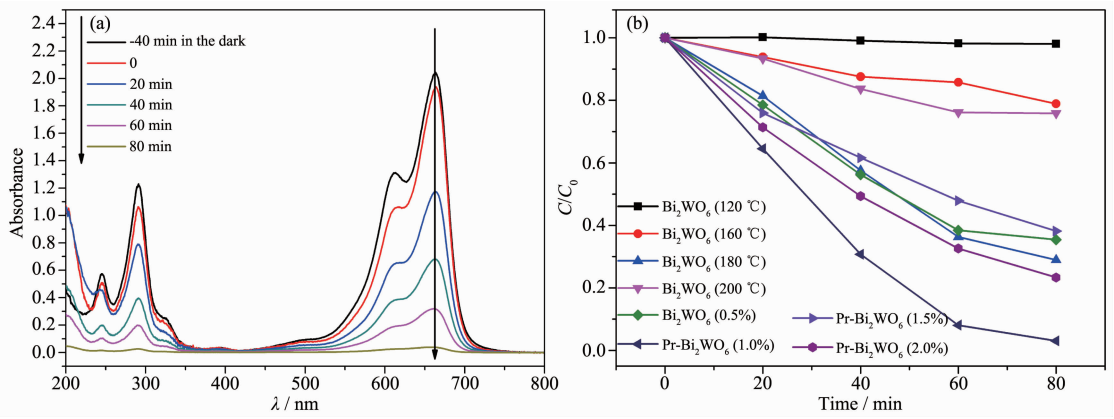

Fig.7 Performance of samples in degradation of the MB solution: (a) UV-Vis spectral changes of the MB solution over 1.0% Pr-Bi_2WO_6 as a function of irradiation time; (b) Changes of concentration of MB solution for different samples

experiments, the MB solution were collected at a degradation time interval of 20 min and then analyzed for total organic carbon (TOC) concentration. The result is shown in Fig.8. In the part of light off, the changes in TOC was observed due to the adsorption of photocatalyst. From Fig.8, the existence of desorption result in the increase of TOC concentration under irradiation with visible light for 20 min. The reduction in TOC generally followed the same trend observed in the MB degradation as discussed earlier (using UV-Vis spectroscopy).

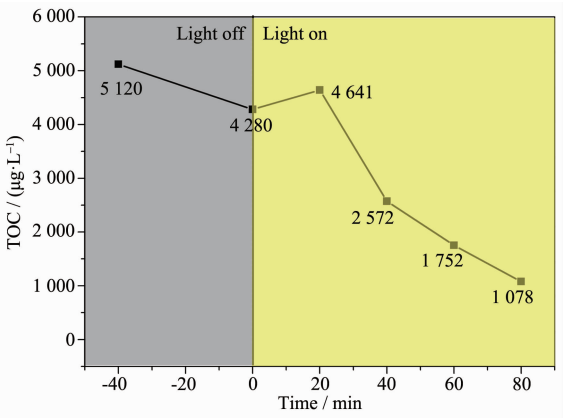

Fig.8 Changes of TOC of MB solution for different reaction time

The high photocatalytic ability of Pr-Bi_2WO_6 should be attributed to the synergistic effect of Pr doping. On the basis of above experimental results and detailed analysis, the possible reaction mechanism is schematically illustrated in Fig.9. Four possible paths of energy transfer approaches are proposed and illustrated in different colors as showing in the Fig.9. A widely held belief of electronic transition is shown as blue route. Under the radiation, electrons are excited from the valence band (Bi6*s* and O2*p*) to its conduction band (W5*d*), leaving the corresponding holes in the valence band[22-23]. The green route shows the preponderance of Pr doping. Many defects are formed after Pr^{3+} ions substitute Bi^{3+}, and free electrons in the bulk and surface of Bi_2WO_6 are captured by the Pr^{3+} ions at the vicinity of defects[3,24]. This green route successfully delays the recombination rate of electron-hole pairs (yellow route). On the other hand, Pr^{3+} could lead to a red-shift of optical absorption edge and generated some levels on the top of valence band[25-26]. These results lead to the occurrence of the red lines. In the end, the degration process can be described as follow: the electrons (e^-) can easily transfer to the oxygen molecules (O_2) adsorbed on the

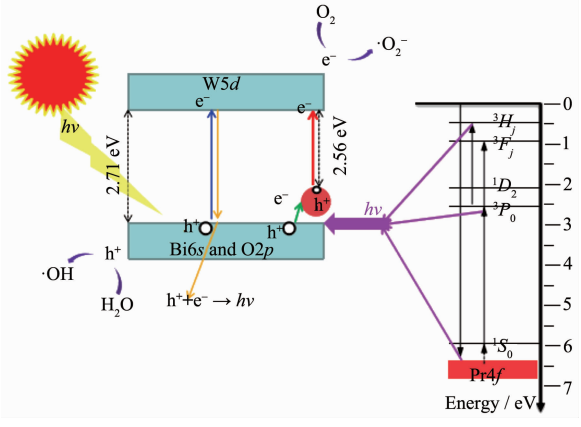

Fig.9 Scheme of photocatalytic mechanism of Pr-Bi_2WO_6

surface of the Bi_2WO_6 photocatalysts, then react with oxygen molecules to generate another active species superoxide radical ($\cdot O_2^-$) for degradation of MB. And the active species of hole (h^+) react with water to generate hydroxyl ($\cdot OH$) or directly oxide organic pollutants[3,25]. Fig.9 also illustrates the energy level scheme of the Pr ion in a compound with small crystal field strength. The crucial step of the cascade emission corresponds to $^1S_0 \rightarrow {}^1I_6$ transitions (a violet line). Next relaxation to the nearest $^3P_0$ level occurs, and the anther important steps, such as $^3P_0 \rightarrow {}^3F_j$ and ^3H_j transitions produces visible emission (main lines near 500 and 600 nm)[27]. These emission energy may be absorbed by photocatalyst, namely pink line in the picture.

Consider the results of three-dimensional flower microspheres shown in Fig.3 and Fig.4, it could be used to predict that the adsorption property make up for the absorbance deficiency of the samples. Furthermore, appropriate content of Pr doped can enhance the photocatalysis possibly due to the separation of electron-hole pairs or the production of some strong oxidative species. Therefore, when optimum amount of Pr doping was 1.0%, the sample exhibit the highest photocatalytic activity for MB.

3 Conclusions

The rare-earth Pr doped Bi_2WO_6 three-dimensional flower microspheres were synthesized successfully by hydrothermal method. The sample of Pr-Bi_2WO_6 prepared at different temperature show different microstructure and the catalyst prepared at 180 ℃ has the best adsorption property and porous structure. These properties can contribute to the photocatalytic degradation. In the meantime, the higher photocatalytic activity is also attributed to the formation of Pr doping, which promote adsorption of visible light and the separation of electron-hole pairs, leading to more active species on the photocatalyst surface. The unambiguous reaction mechanisms for photocatalysis in this work should offer some case for the future development of rare earth doping photocatalyst.

Acknowledgments: This work is financially supported by the Project Sponsored by the Scientific Research Foundation for the Returned Overseas Chinese Scholars, State Education Ministry, Natural Science Foundation of the Jiangsu Higher Education Institutions of China (Grants No.14KJB430023 and 15KJA430007), Jiangsu Collaborative Innovation Center for Ecological Building Materials and Environmental Protection Equipments (Grants No.CP201502 and GX2015102), Natural Science Foundation of Jiangsu Province (Grant No.BK20140472) and College Students′ Innovative Entrepreneurial Training Plane of Colleges and Universities in Jiangsu Province (Grant No. 201610305002Z).

Author Contributions: ZHANG Ya-Heng conceived and designed the experiments; ZHAI Ren-Kai and LI Jian-Xing performed the experiments; XI Xin-Guo and ZHANG Ya-Heng contributed materials and tools; TIAN Hao and GU Da-Guo analyzed the data and ZHANG Ya-Heng, TIAN Hao and QIANG Gui-Hong wrote the paper.

Conflicts of Interest: The authors declare no conflicts of interest.

References:

[1] Hoffmann M R, Martin S T, Choi W, et al. *Chem. Rev.*, **1995**, **95**:69-96

[2] Wang H, Zhang L, Chen Z, et al. *Chem. Soc. Rev.*, **2014**,**43**: 5234-5244

[3] Tian N, Zhang Y H, Huang H W, et al. *J. Phys. Chem. C*, **2014**,**118**:15640-15648

[4] Fu Y, Chang C, Chen P, et al. *J. Hazard. Mater.*, **2013**,**254-255**:185-192

[5] Xiao Q, Si Z, Zhang J, et al. *J. Hazard. Mater.*, **2008**,**150**:62-67

[6] Fan N Y, Hou H G, Feng Q M, et al. *Chin. J. Lumin.*, **2012**, **3**:263-267

[7] Obregon S, Colon G. *Appl. Catal., B*, **2014**,**152**:328-334

[8] Adhikari R, Gyawali G, Cho S H, et al. *J. Solid State Chem.*, **2014**,**209**:74-81

[9] Zhang W H, Yuan N, Zhang L S, et al. *Mater. Lett.*, **2016**, **163**:16-19

[10]Zhang J, Huang Z H, Xu Y, et al. *Int. J. Photoenergy*, **2012**: 469178(12 pages)

[11]Shang M, Wang W Z, Sun S M, et al. *J. Phys. Chem. C*, **2008**,**28**:10407-10411

[12]Singh A, Dutta D P, Roy M, et al. *J. Mater. Sci.*, **2014**,**5**:

2085-2097

[13]DONG Wei-Xi(董伟霞), BAO Qi-Fu(包启福), GU Xing-Yong(顾幸勇), et al. *Chinese J. Inorg. Chem.*(无机化学学报), **2017**,**33**(2):292-298

[14]Dong P Y, Wang Y H, Cao B C, et al. *Appl. Catal., B*, **2013**, **132-133**:45-53

[15]Tong H, Ouyang S, Bi Y, et al. *Adv. Mater.*, **2012**,**24**:229-251

[16]Greg S, Sing K. *Adsorption, Surface Area and Porosity*. 2*nd Ed*. London: Academic Press, **1982**.

[17]Dong P Y, Wang Y H, Liu B, et al. *Appl. Surf. Sci.*, **2012**, **258**:7052-7058

[18]Tsunekawa S, Fukuda T, Kasuya A. *J. Appl. Phys.*, **2000**, **87**:1318-1321

[19]Yayapao O, Thongtem T, Phuruangrat A, et al. *J. Alloys Compd.*, **2011**,**509**:2294-2299

[20]Liu Y, Wang W M, Fu Z Y, et al. *Mater. Sci. Eng., B*, **2011**,**176**:1264-1270

[21]YAN Xin(阎鑫), HUI Xiao-Yan(惠小燕), GAO Qiang(高强), et al. *Chinese J. Inorg. Chem.*(无机化学学报), **2017**,**33**(10): 1782-1788

[22]Zhu Z F, Yan Y, Li J Q. *J. Alloys Compd.*, **2015**,**651**:184-192

[23]Phuruangrat A, Maneechote A, Dumrongrojthanath P, et al. *Mater. Lett.*, **2015**,**159**:289-292

[24]Zhang W H, Yuan N, Zhang L S, et al. *Mater. Lett.*, **2016**, **163**:16-19

[25]Zhang Y, Ma Y, Liu Q, et al. *Ceram. Int.*, **2017**,**2**:2598-2605

[26]Jiang H Y, Liu J, Cheng K, et al. *J. Phys. Chem. C*, **2013**, **117**:20029-20037

[27]Rodnyi P A, Mikhrin S B, Dorenbos P, et al. *Opt. Commun.*, **2002**,**204**:237-245